β-Cyclodextrin modified Pt(II) metallacycle-based supramolecular hyperbranched polymer assemblies for DOX delivery to liver cancer cells

Wenzhuo Chen[a,b,1], Xuefeng Li[c,d,e,1], Chengfei Liu[a], Jia He[a], Miao Qi[a], Yue Sun[b], Bingbing Shi[b], Hajar Sepehrpour[b], Hui Li[f], Wei Tian[a,2], and Peter J. Stang[b,2]

[a]Shaanxi Key Laboratory of Macromolecular Science and Technology, Ministry of Education Key Laboratory of Material Physics and Chemistry under Extraordinary Conditions, School of Chemistry and Chemical Engineering, Northwestern Polytechnical University, 710072 Xi'an, China; [b]Department of Chemistry, University of Utah, Salt Lake City, UT 84112; [c]The Sixth Affiliated Hospital of Guangzhou Medical University, Qingyuan People's Hospital; State Key Laboratory of Respiratory Disease, Sino-French Hoffmann Institute, School of Basic Medical Sciences, Guangzhou Medical University, 511436 Guangzhou, People's Republic of China; [d]Shenzhen Luohu People's Hospital, The Third Affiliated Hospital of Shenzhen University, 518001 Shenzhen, People's Republic of China; [e]Key Laboratory of Regenerative Biology, Guangdong Provincial Key Laboratory of Stem Cell and Regenerative Medicine, South China Institute for Stem Cell Biology and Regenerative Medicine, Guangzhou Institutes of Biomedicine and Health, Chinese Academy of Sciences, 510530 Guangzhou, People's Republic of China; and [f]School of Materials Science and Engineering, Jiangxi University of Science and Technology, 341000 Ganzhou, People's Republic of China

Contributed by Peter J. Stang, May 27, 2020 (sent for review April 23, 2020; reviewed by Harry B. Gray and Jean-Marie P. Lehn)

Despite the widespread clinical application of chemotherapeutic anticancer drugs, their adverse side effects and inefficient performances remain ongoing issues. A drug delivery system (DDS) designed for a specific cancer may therefore overcome the drawbacks of single chemotherapeutic drugs and provide precise and synergistical cancer treatment by introducing exclusive stimulus responsiveness and combined chemotherapy properties. Herein, we report the design and synthesis of a supramolecular drug delivery assembly 1 constructed by orthogonal self-assembly technique in aqueous media specifically for application in liver cancer therapy. Complex 1 incorporates the β-cyclodextrin host molecule-functionalized organoplatinum(II) metallacycle 2 with two specific stimulus-responsive motifs to the signaling molecule nitric oxide (NO), in addition to the three-armed polyethylene glycol (PEG) functionalized ferrocene 3 with redox responsiveness. With this molecular design, the particularly low critical aggregation concentration (CAC) of assembly 1 allowed encapsulation of the commercial anticancer drug doxorubicin (DOX). Controlled drug release was also achieved by morphological transfer via a sensitive response to the endogenous redox and NO stimuli, which are specifically related to the microenvironment of liver tumor cells. Upon combination of these properties with the anticancer ability from the platinum acceptor, in vitro studies demonstrated that DOX-loaded 1 is able to codeliver anticancer drugs and exhibit therapeutic effectiveness to liver tumor sites via a synergistic effect, thereby revealing a potential DDS platform for precise liver cancer therapeutics.

supramolecular coordination complex | drug delivery system | supramolecular hyperbranched polymer assemblies | metallacycle | combination chemotherapy

The spontaneous formation of metal–ligand bonds is the basis of the well-established coordination-driven self-assembly methodology for the construction of supramolecular coordination complexes (SCCs). Well-defined and therapeutic SCCs metallacycles can be prepared using metal acceptors and organic donors due to the facile functionalization of these secondary recognition moieties (1–7). By introducing platinum-based acceptors with anticancer activities, Pt(II) metallacycle-based SCCs have been proven to act as antitumor agents, in addition to exhibiting the potential to behave as scaffolds to build combination treatment platforms (8–14). However, to overcome the resistance and selectivity limitations of platinum-based anticancer drugs, a cancer-specific drug delivery system (DDS) composed of Pt-based SCCs would be of particular interest.

During the past few decades, supramolecular polymer assemblies have aroused attention as DDSs for cancer therapeutics (15–19). Indeed, such a noncovalent approach can greatly alleviate the difficulties and labor associated with the organic syntheses of complicated structures. In addition, the building blocks and the corresponding functions of the intrinsic responsive systems can be easily achieved by dynamic and reversible noncovalent strategies. Most importantly, chemical, physical, and biological properties may be enhanced due to the hyperbranched topological structures of supramolecular polymer (20–22). However, the most frequently used internal stimuli in supramolecular DDSs (e.g., pH, redox properties and enzymes) have inherent limitations in terms of the release of anticancer therapeutic reagents, since local environments vary between different kinds of cancers. Since few supramolecular polymer bearing hyperbranched topological structures for the application of DDSs have been reported (23–25), the development of supramolecular hyperbranched polymer assemblies constructed DDSs

Significance

The development of chemotherapeutic drugs for cancer treatment has been limited by problems such as adverse side effects and inefficient performance of the drugs. To deliver multiple anticancer drugs for accurate and synergistic liver cancer treatment, a Pt(II) metallacycle-based drug delivery system, with endogenous redox and nitric oxide stimuli responsiveness and two chemotherapeutic agents is designed via the orthogonal self-assembly strategy. In vitro studies demonstrate that this system has good ability to deliver hydrophobic anticancer drug doxorubicin to HepG2 liver cancer cells. It also efficiently inhibits tumor cell growth for enhanced liver cancer treatment. This study provides an opportunity for the further design of metallacycle-based drug delivery systems for cancer therapy.

Author contributions: W.C., W.T., and P.J.S. designed research; W.C., X.L., C.L., and J.H. performed research; W.C., M.Q., Y.S., B.S., H.S., W.T., and P.J.S. contributed new reagents/analytic tools; W.C., X.L., Y.S., B.S., H.L., W.T., and P.J.S. analyzed data; and W.C., X.L., W.T., and P.J.S. wrote the paper.

Reviewers: H.B.G., California Institute of Technology; and J.-M.P.L., University of Strasbourg.

The authors declare no competing interest.

[1]W.Z. and X.L. contributed equally to this work.

[2]To whom correspondence may be addressed. Email: happytw_3000@nwpu.edu.cn or stang@chem.utah.edu.

This article contains supporting information online at https://www.pnas.org/lookup/suppl/doi:10.1073/pnas.2007798117/-/DCSupplemental.

First published November 23, 2020.

exhibiting highly sensitive endogenous stimulus responsiveness to specific cancer lines is of particular interest.

Nitric oxide (NO) is a biological signaling molecule that plays a key role in many physiological and pathological processes. Notably, in liver cancer pathophysiology, the inducible nitric oxide synthase, located in the cytosol of liver cancer cells, can produce large quantities of NO, which can form reactive nitrogen species that in turn damage the DNA, lipids, and proteins (26–32). As a result, nitric oxide can be employed as a new kind of endogenous stimuli-responsiveness factor with the potential for contributing to drug control and release in the context of liver cancers. In addition, the formation of robust metal–ligand bonds can take place in parallel with other intermolecular interactions, thereby allowing the construction of superior topologies in an orthogonal self-assembly manner (33–35). Thus, we herein report the design and synthesis of supramolecular complex **1**, which incorporates the β-cyclodextrin (β-CD) host molecule-functionalized organoplatinum(II) metallacycle **2** with unique NO responsiveness, and the three-arm PEGylated ferrocene **3** exhibiting redox responsiveness, which can be prepared via orthogonal coordination-driven self-assembly and cyclodextrin-based host–guest interactions (Fig. 1). Due to this design, **1** can further form a spherical nanoparticle of a specific size and a particularly low critical aggregation concentration (CAC) in water. The ability of assembly **1** to encapsulate the commercial anticancer drug doxorubicin (DOX) in its hydrophobic cavity is also investigated, along with the ability of the acceptor moiety of **2**, 3,6-bis[trans-Pt(PEt_3)$_2$]phenanthrene to act as a chemotherapeutic agent. These properties would ultimately endow assembly **1** with enhanced anticancer ability for combination chemotherapy. In addition, precise controlled drug release is examined via the response of assembly **1** to the endogenous NO and redox stimuli that are specific to the microenvironment of liver tumor cells. Furthermore, we expect that the β-CD and three-arm PEGylated ferrocene moeities will serve as hyperbranched building blocks to enhance the stability and biocompatibility of assembly **1**. To further verify the synergistic therapeutics based on assembly **1** are achieved, in vitro studies are carried out to demonstrate the cellular internalization of DOX-loaded **1**, in addition to the DOX delivery efficiency, and the efficacy to kill HepG2 liver cancer cells compared with DOX alone. Ultimately we wish to demonstrate the potential of assembly **1** as a DDS platform for precise liver cancer chemotherapeutics.

Results and Discussion

According to the principle of directional bonding, the directionality and angularity of each component involved in coordination-driven self-assembly dictate the final architectural outcome, wherein discrete SCCs with well-defined shapes, sizes, and functional groups, can be easily prepared in high efficiencies. In this study, the 120° bipyridyl ligand **4** bearing the β-CD host and the highly NO-reactive amide-functionalized *o*-phenylenediamine moiety was initially synthesized via a Pd-catalyzed Suzuki coupling reaction, an amidation reaction, and a copper(I)-catalyzed click reaction (*SI Appendix*, Scheme S1), and was fully characterized by ^{1}H and ^{13}C NMR spectroscopy in addition to mass spectrometry (*SI Appendix*, Figs. S1–S15). Subsequently, the 120° bipyridyl ligand **4** and 60° di-Pt(II) acceptor **5** (PhenPt) were combined to furnish rhomboidal **2**. More specifically, a mixture of **4** and **5** in a 1:1 ratio in dimethyl sulfoxide stirred at 20 °C for 3 h led to the formation of the self-assembled [2 + 2] rhomboidal **2** (Fig. 1*A*). Characterization by ^{1}H and ^{31}P{^{1}H} NMR spectroscopy in addition to electrospray ionization time-of-flight mass spectrometry (ESI-TOF-MS) established the successful construction of **2**. Upon the formation of **2**, the ^{31}P{^{1}H} NMR signal was shifted significantly upfield from those of the starting Pt(II) acceptor **5** by ~5.52 ppm, and a lone sharp singlet was observed at ~14.60 ppm with concomitant ^{195}Pt satellites (J_{Pt-P} = 2,679.5 Hz), consistent with a single phosphorus environment (Fig. 2*A*). Likewise, the ^{1}H NMR signals observed between 7.0 and 9.3 ppm were characteristic of the metallacycle (*SI Appendix*, Fig. S16). The NMR results therefore confirmed the formation of a discrete structure as the sole isolated assembled product.

ESI-TOF-MS is a highly reliable tool to provide evidence for the stoichiometries of multicharged supramolecular structures. Thus, the stoichiometry of **2** was verified by ESI-TOF-MS. As shown in Fig. 2*B* and *SI Appendix*, Fig. S17, the isotopically resolved peaks corresponding to the intact metallacycle with the loss of trifluoromethanesulfonate (OTf) anions were observed at *m*/*z* 1,309.2039 for $[M-4OTf]^{4+}$. The isotopic spacings of these peaks were in good agreement with their theoretical distributions, thereby confirming the successful preparation of the di-β-CD–modified platinum-based rhomboidal metallacycle.

It is well-known that β-CD can complex with ferrocene groups to form stable host–guest complexes (36–38). Thus, to improve the possibility of the application of **2** in the treatment of liver cancer, precursor **3**, bearing three-armed PEGylated ferrocene, were synthesized (*SI Appendix*, Scheme S3 and Figs. S18–S22), and supramolecular complex **1** was constructed in water by simply mixing **2** and **3**. Fluorescence probe measurements were then performed in aqueous solution to determine the CAC. More specifically, following the dissolution of **2** in water in the presence of 0.67 equiv. **3**, the fluorescent changes in the pyrene probe were used to determine the CAC value of complex **1**. The observed two linear segments in the curve and a sudden enlargement of the slope indicated that the CAC value of 1 is ~2.7 μg/mL (*SI Appendix*, Fig. S23). Subsequently, the supramolecular self-assembly behaviors of **2** and host–guest complex **1** were investigated in aqueous solution. Transmission electron microscopy (TEM) and scanning electron microscopy (SEM) experiments allowed visualization of the self-assembled nanostructures. More specifically, Fig. 3*A* shows the TEM micrograph of **2**, whereby its self-assembly into nanoparticles with diameters of approximately tens of nanometers was confirmed. The noncovalent host–guest assembly **1** was then formed upon the addition of 0.67 equiv. of **3** to **2.** Following dilution to ~20 μM, spherical nanoparticles with an average diameter of ~300 nm were formed (Fig. 3*B*). Similar spherical structures of ~300 nm in diameter were also observed by SEM (Fig. 3*C*), likely due to their aggregated morphological features. Furthermore, dynamic light-scattering (DLS) experiments produced results that were indirectly consistent with the morphology observed by TEM and SEM, thereby suggesting that the diameter of assembly **1** ranged from 100 to 600 nm, with a relatively broad size distribution (Fig. 3*D*). Indeed, similar concentration-dependent morphological variations of metallacycle-cored supramolecuar complexes have been reported recently (39, 40). Moreover, high-angle annular dark field-scanning transmission electron microscopy (HAADF-STEM) images of the elemental distributions in the spherical nanoparticles confirmed the presence of platinum, phosphorus, iron, carbon, nitrogen, and oxygen in the assemblies of **1** (Fig. 3 *E*–*K*). These results therefore confirm preparation of the desired self-assembled nanospheres for subsequent investigation into their potential application as DDSs.

In addition to the incorporation of amide-functionalized *o*-phenylenediamine sites in **2** that can be cleaved by the reaction with NO in aqueous media (41, 42), **3** contains ferrocene groups that can detach from the β-CD moieties under an oxidizing atmosphere to achieve redox responsiveness (43–45). Thus, to verify the NO/redox responsiveness of **1**, TEM was employed to study the morphological changes after exposure to NO/H_2O_2. As shown in Fig. 4*B*, following the addition of an excess quantity of NO to a solution of assemblies of **1**, the TEM images obtained after 4 h indicated that the globular assemblies of **1** gradually collapsed into smaller striplike aggregates, likely indicating a

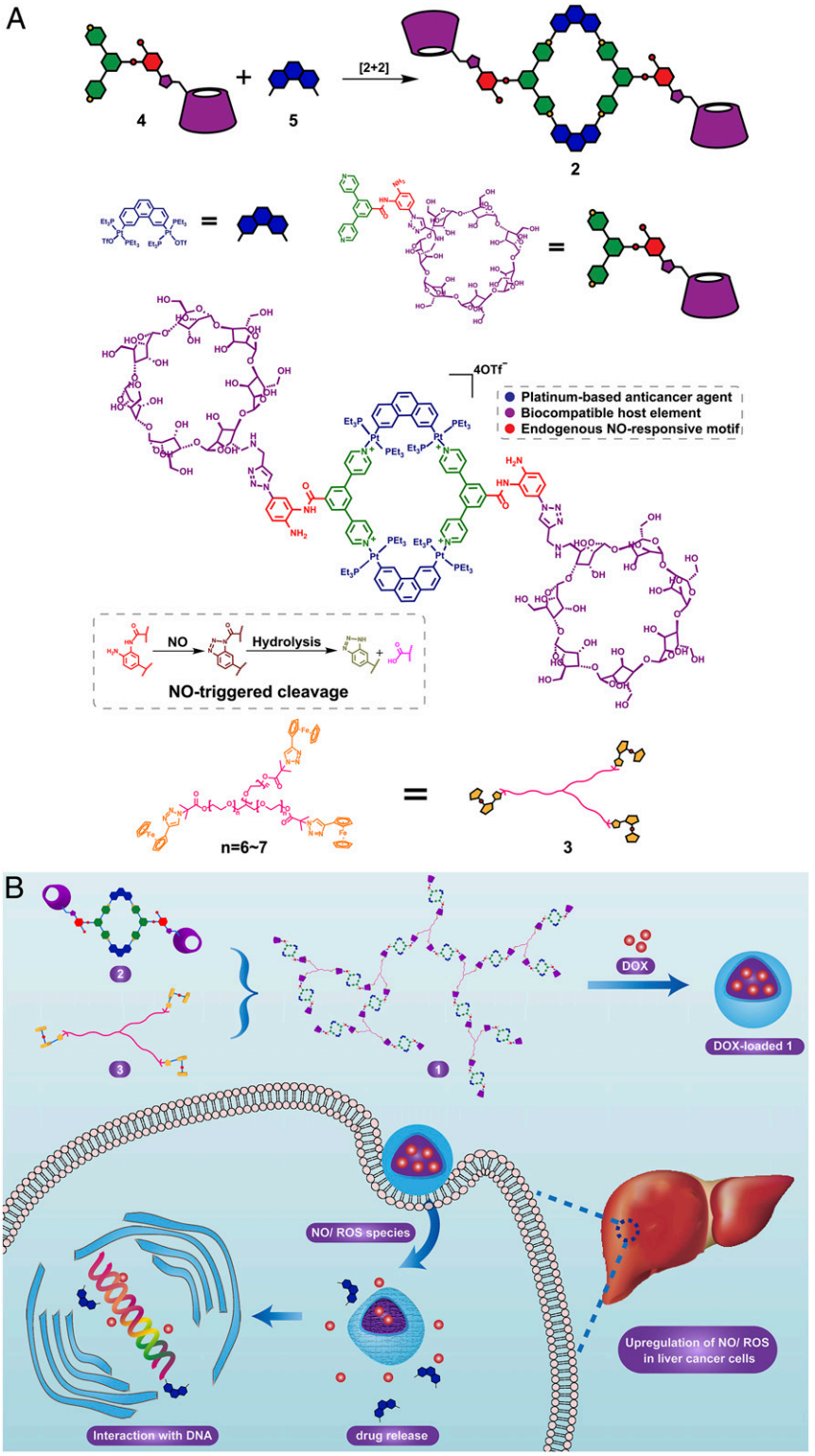

Fig. 1. (*A*) Synthesis of **2** and its NO-triggered cleavage mechanism. (*B*) Cartoon illustration of the cellular uptake of DOX-loaded nanostructures self-assembled from **1**.

partial cleavage of the amide-functionalized *o*-phenylenediamine units. Ultraviolet (UV)-vis spectrophotometric investigations also showed variations upon the addition of NO, which were similar to those described in a previous report (*SI Appendix*, Figs. S24–S26). Upon prolonging the incubation time from 8 to 24 h (Fig. 4 *C* and *D*), complete disassembly of the spherical structures and the reassociation of larger irregular nanostructures measuring a few micrometers were observed. These processes were also monitored via DLS (Fig. 4 *A* and *E*), and the results were in agreement with the TEM observations, thereby revealing the NO responsiveness and morphological transformation of **5**. Similar results were obtained with the addition of H_2O_2,

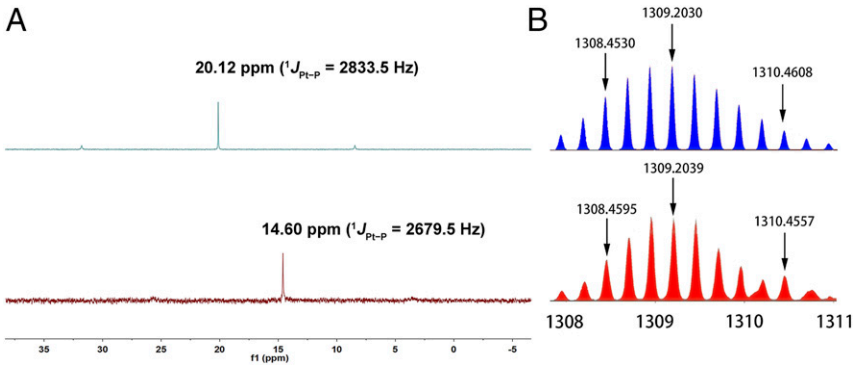

Fig. 2. (*A*) ^{31}P NMR spectra (methanol-d_4, 293 K, 121.4 MHz) of 60° acceptor **5** and metallacycle **2**. (*B*) Experimental (blue) and calculated (red) electrospray ionization peaks of the $[M - 4OTf]^{4+}$ charge states of **2**.

whereby partial collapse of the globular nanoparticles and the formation of small nanoparticles were observed after 4 h, likely due to dissociation of the positively charged ferrocene units from the β-CD cavities. Upon extending the incubation time to 24 h, micrometer-scale irregularities were generated once again, and UV-vis variation curve according to different concentration of NO and time were also obtained. (*SI Appendix*, Figs. S24–S26). The NO and redox responsive-induced morphological changes

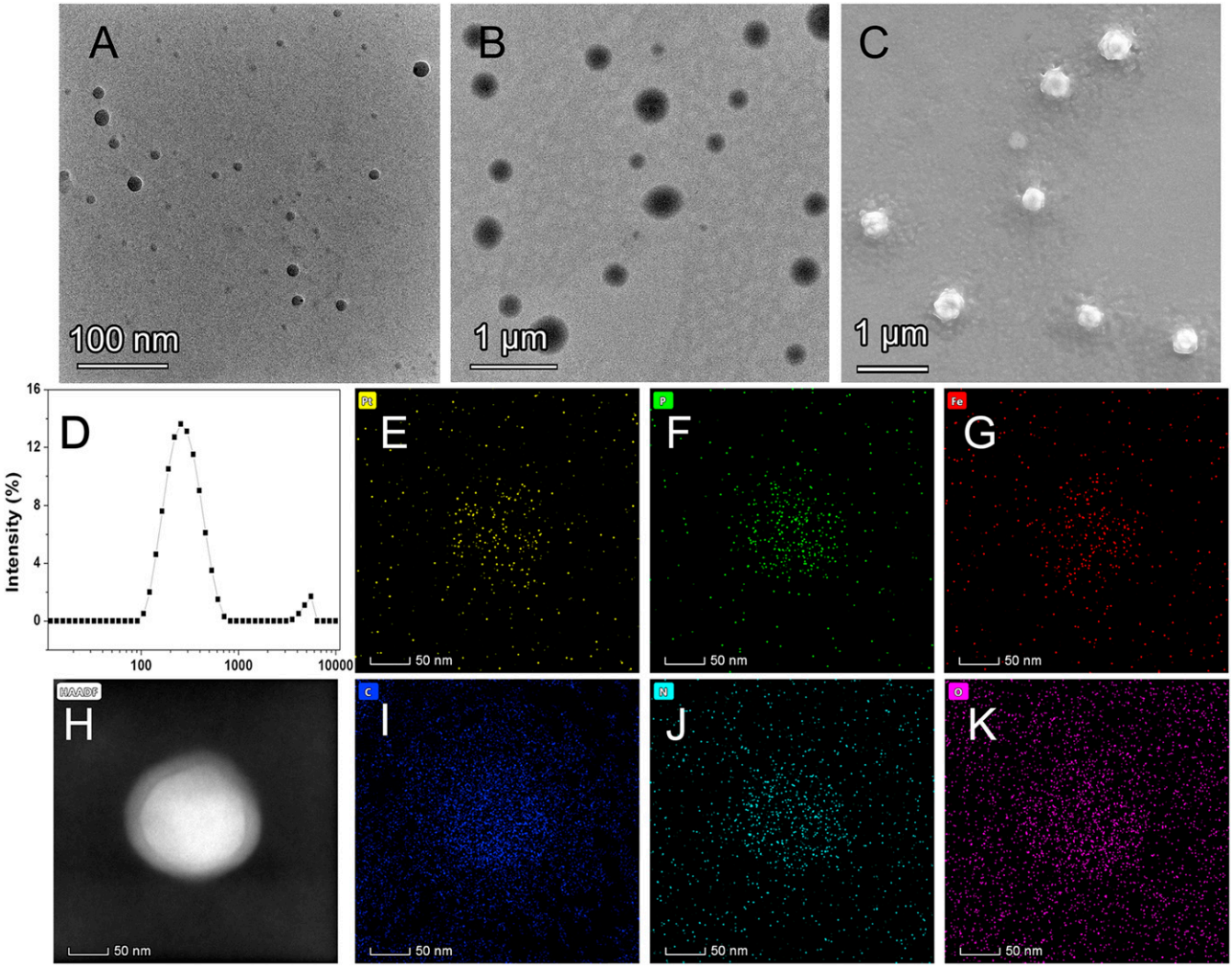

Fig. 3. TEM images of self-assembled nanostructures obtained from aq. solutions of (*A*) **2** at a concentration of 12 μM. (*B*) **1** at concentrations of 20 μM. (*C*) SEM images of **1** at concentrations of 20 μM. (*D*) The average diameters of 1 at a concentration of 20 μM were determined by DLS. (*E–K*) HAADF-STEM images of elements distribution of **1**.

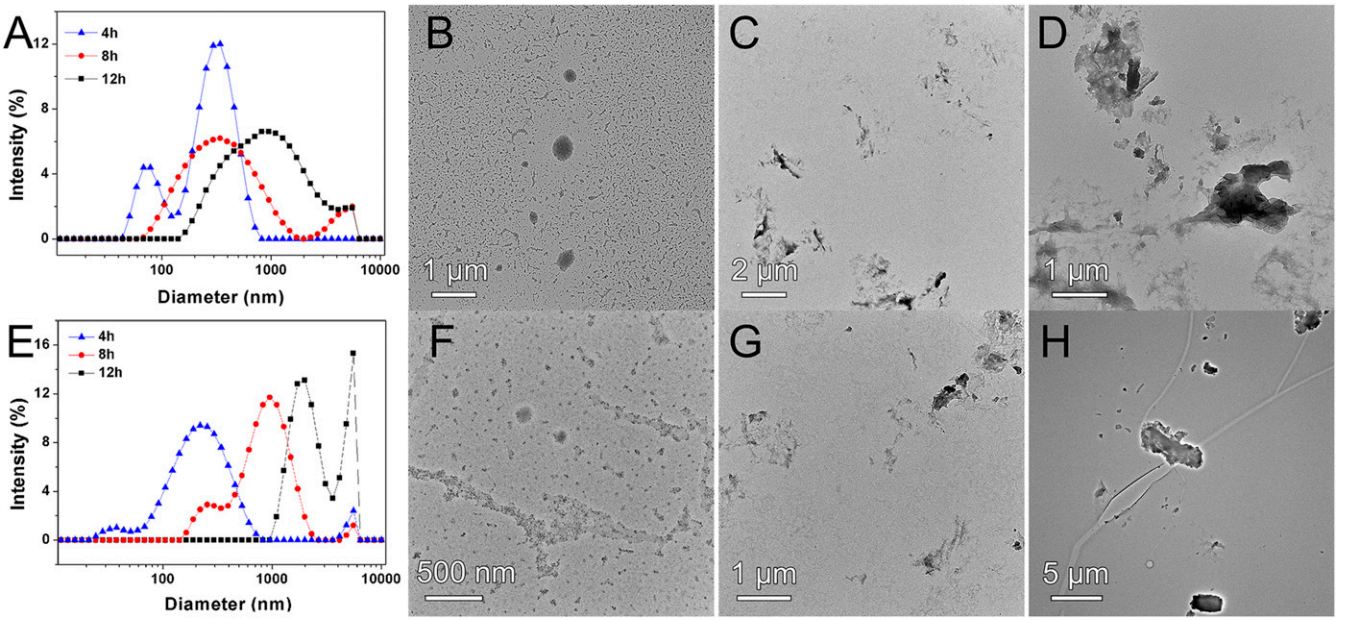

Fig. 4. Particle-size distribution of **1** after treatment with (*A*) NO, (*E*) H_2O_2. (*B–D*) TEM images of 5 after treatment with NO for 4, 8, 24 h, respectively. (*F–H*) TEM images of **1** after treatment with H_2O_2 for 4, 8, 24 h, respectively.

of this delivery system were therefore apparent from the described results.

With the NO/redox-responsive supramolecular self-assembly in hand, the corresponding self-assembled nanoparticles **1** were then investigated as potential DDSs in the controlled release of small anticancer drugs for combination chemotherapy. The hydrophobic anticancer drug DOX is suitable to be loaded into the assembly **1** with hydrophobic cavities to measure the encapsulation efficiency and release behavior of the assembly **1**. Initially, the encapsulation of DOX was carried out via reprecipitation and dialysis method. The encapsulation efficiency was subsequently studied by UV-vis spectroscopy, and the drug loading was calculated to be 23.95% (*SI Appendix*, Fig. S27). The effective DOX loading capacity of assembly **1** might be attributed to multiple noncovalent interactions such as the hydrophobic interaction, π–π stacking interaction, host–guest interaction, and other interactions between DOX and assembly **1** (11, 46–48). In addition, no obvious size variation was detected by DLS in phosphate buffer saline containing 10% fetal bovine serum at pH 7.4 over 72 h (*SI Appendix*, Fig. S28). The release profiles of the DOX-loaded **1** were then investigated using a dialysis method through measurement of the DOX content by UV-vis spectroscopy at 37 °C in PBS. As shown in Fig. 5*A*, in the absence of NO/H_2O_2 stimuli, DOX-loaded **1** exhibited <15% release of DOX over 48 h, indicating that the nanoparticles are relatively stable toward leakage under these physiological conditions. Following the addition of ∼50 μM NO to the solution of DOX-loaded nanoparticles, the DOX release rate was accelerated due to the NO-triggered cleavage of the amide-functionalized *o*-phenylenediamine units of **2**, resulting in ∼13.7% release over the first 4 h, and 41.2% within 24 h. In addition, the release of DOX induced by 50 μM H_2O_2 was confirmed as shown in Fig. 5, whereby the obtained release profiles indicated that 48.3% of DOX could be released slowly over 48 h. As a result, this smooth release phenomenon, which confirmed a good response to relatively high concentrations of endogenous NO and H_2O_2 in the liver tumor microenvironment, indicated that DOX-loaded **1** demonstrated controllable DOX release, and therefore appeared to act as an ideal candidate for a DDS.

To further investigate the cellular uptake of the NO/redox-responsive drug release system based on **1**, the cellular internalization of the DOX-loaded nanoparticles by HepG2 liver cancer cells was examined by confocal laser scanning microscopy (CLSM). As shown in Fig. 5 *B–F*, the HepG2 cells were treated with both naked DOX·HCl and DOX-loaded nanoparticles **1** for up to 6 h. Compared with the naked DOX·HCl group, higher intensities of red fluorescence related to DOX were observed in the cytoplasm and nucleus of HepG2 cells after treatment with DOX-loaded **1**. We suppose the delivery might go through classic endocytosis pathway (49). Although we did not detect the colocalization of endosome with DOX-loaded 1, and whether it is clathrin-dependent nor non–clathrin-dependent endocytosis (50). Nonetheless, the results indicate efficient DOX delivery and accelerated release due to the relatively higher levels of NO and oxidative stress that are associated with liver cancers. Moreover, a simple evaluation of the cytotoxicities and anticancer efficiencies for **1**, **2**, **3**, and DOX-loaded **1** at different concentrations against HepG2 were performed using the 3-(4,5-dimethylthiazol-2-yl)-2,5-diphenyltetrazolium bromide assay, wherein cells treated with the free DOX·HCl or a blank PBS solution were used as the control group. As shown in Fig. 5*G*, following incubation for 24 h at 37 °C in PBS solution, no apparent toxicity was observed for precursor **3**, even at a concentration of 50 μM. Assembly **1**, platinum-based metallacycle **2**, and the naked DOX·HCl all exhibited good anticancer activities against the HepG2 cells, likely due to the coordination ability of the Pt centers and DOX to the DNA of the HepG2 cells. However, compared with the free DOX·HCl, preferable growth inhibition was observed for the cells incubated with DOX-loaded **1**, even at lower concentrations (10 μM). This was attributed to the synergistic effect of the NO/H_2O_2 dual-responsive controlled release of the two chemotherapeutic agents, namely DOX and PhenPt. These observations indicate that the present system presents a high cytotoxicity to HepG2, and that it also appears suitable for the specific delivery of chemotherapeutic agents (i.e., DOX) into liver cancer cells for a combined chemotherapy approach.

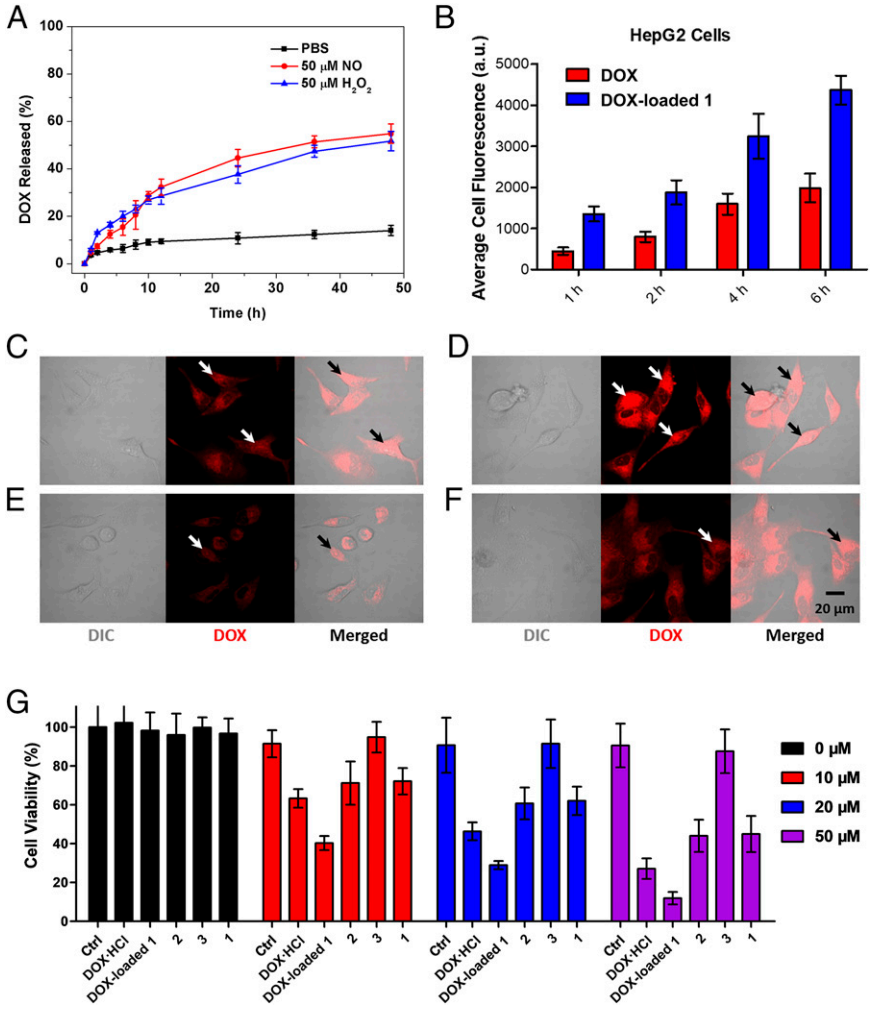

Fig. 5. (*A*) Time-dependent release of DOX from DOX-loaded **1** after treatment with 50 μM NO/H_2O_2. (*B*) Detection of DOX release intensity and rate by confocal microscopy (Zeiss LSM 810). DOX fluorescence images of HepG2 cells incubated with or without DOX-loaded **1** for 1–6 h at 37 °C. Average cell fluorescence of HepG2 cells is obtained by the average fluorescence intensity from 100 cells in each DOX fluorescence image at different times. Means ± SD from triplication. (*C–F*) Dox images were taken with exposure for 100 ms and 481-nm excitation wavelength using the DOX fluorescence microscope at 63× magnification, respectively: (*C*) DOX-loaded **1**, 1 h; (*D*), DOX-loaded **1**, 6 h; (*E*) DOX, 1 h; (*F*), DOX, 6 h). Data are representative from three independent experiments. (Scale bar = 20 μm.) (*G*) Cellular toxicity of DOX, DOX-loaded **1**, **2**, **3**, and **1** on HepG2 cells.

Conclusion

In conclusion, a β-CD-functionalized organoplatinum(II) metallacycle **2** exhibiting NO responsiveness was successfully synthesized through organoplatinum(II) coordination-driven self-assembly. Following the addition of three-arm PEGylated ferrocene **3** to a solution of **2**, a supramolecular complex **1** was successfully constructed due to the host–guest interactions between the β-CD and ferrocene groups. The resulting supramolecular complex was then found to self-assemble into spherical nanoparticles with diameters of ∼300 nm at low concentrations in aqueous solution. In addition, these nanoparticles exhibited sensitive endogenous NO/redox responsiveness, and spontaneously transformed into irregular structures following the addition of NO to their solutions due to cleavage of the amide-functionalized *o*-phenylenediamine units of **2** by NO. Similarly, the redox responsiveness was demonstrated through the detachment of ferrocene from the CD cavities upon the addition of an oxidizing agent such as H_2O_2. Importantly, it was demonstrated that the anticancer drug DOX could be successfully encapsulated into the cavity of the resultant nanoparticles of **1**. Upon the addition of NO/H_2O_2 to the drug-loaded nanoparticle solution, accelerated collapse of the spherical structure and release of the drugs encapsulated in the nanoparticles were observed. Thus, combination of the exclusive stimulus responsiveness to liver tumor microenvironment and the anticancer ability of both DOX and platinum acceptor allowed in vitro experiments to demonstrate that **1** can exhibit an improved DOX delivery and enhanced therapeutic efficacy via a synergistic effect. This work therefore provides valuable information regarding the elaborate design of metallacycle-based drug DDSs for application in liver cancer therapeutics.

Materials and Methods

The ^{1}H and ^{13}C NMR spectra were acquired on a Bruker 400-MHz magnetic resonance spectrometer. The 31P{1H} NMR spectra were recorded on a Varian Unity 300-MHz spectrometer. Electrospray-ionization time-of-flight mass spectrometry analyses were performed on an Applied Biosystems 4700 matrix-assisted laser desorption-ionization time-of-flight mass spectrometer. UV-vis spectra were measured by using an Agilent Cary-100 spectrophotometer. Hydrodynamic diameter was measured by using a Zeta sizer Nano ZS90 before sample was filtered. High performance liquid chromatography was performed on a Dionex HPLC System (Dionex Corporation) and a reversed-phase C18 column was used for semipreparation (Agilent, 5 μm, 10 mm × 250 mm). The sample for TEM and HAADF-scanning

transmission electron microscopy (HAADF-STEM) was prepared by dropping the solution onto a copper grid and the sample was examined by an FEI Talos F200X instrument. SEM was carried out using Verios G4 microscope.

Data Availability. The details of the synthesis, characterization, and biological experiments are given in *SI Appendix*.

ACKNOWLEDGMENTS. This work was supported by National Natural Science Foundation of China Grants 22071197, 22022107, 21674086, Natural Science Basic Research Plan in Shaanxi Province of China Grant 2020JC-20/2018JZ2003, and Fundamental Research Funds for the Central Universities Grant 3102019PY003 (to W.T.); National Natural Science Foundation of China Grants 81972204 and 81702327, China Postdoctoral Science Foundation Grants 2018M640834 and 2019T120756, Innovation Program of Shenzhen Grant JCYJ20180508165208399, Science and Technology Planning Project of Guangzhou Grant 201904010089, the State Key Laboratory of Respiratory Disease, Guangzhou Medical University Grant SKLRD-Z-202002, and the 111 Project from the Ministry of Education of China Grant D18010 (to X.L.); China Scholarships Council Grant 201706290162 (to W.C.). We especially thank Prof. Xiaopeng Li and Dr. Ruidong Ni from Department of Chemistry, University of South Florida for mass spectrometry testing and analysis. The authors also thank the Analytical & Testing Center of Northwestern Polytechnical University for electron microscope tests.

1. N. N. Adarsh, P. Dastidar, Coordination polymers: What has been achieved in going from innocent 4,4′-bipyridine to bis-pyridyl ligands having a non-innocent backbone? *Chem. Soc. Rev.* **41**, 3039–3060 (2012).
2. R. Chakrabarty, P. S. Mukherjee, P. J. Stang, Supramolecular coordination: Self-assembly of finite two- and three-dimensional ensembles. *Chem. Rev.* **111**, 6810–6918 (2011).
3. T. R. Cook, Y.-R. Zheng, P. J. Stang, Metal-organic frameworks and self-assembled supramolecular coordination complexes: Comparing and contrasting the design, synthesis, and functionality of metal-organic materials. *Chem. Rev.* **113**, 734–777 (2013).
4. S. De, K. Mahata, M. Schmittel, Metal-coordination-driven dynamic heteroleptic architectures. *Chem. Soc. Rev.* **39**, 1555–1575 (2010).
5. M. Fujita, M. Tominaga, A. Hori, B. Therrien, Coordination assemblies from a Pd(II)-cornered square complex. *Acc. Chem. Res.* **38**, 369–378 (2005).
6. L. E. Kreno *et al*., Metal-organic framework materials as chemical sensors. *Chem. Rev.* **112**, 1105–1125 (2012).
7. B. H. Northrop, Y.-R. Zheng, K.-W. Chi, P. J. Stang, Self-organization in coordination-driven self-assembly. *Acc. Chem. Res.* **42**, 1554–1563 (2009).
8. I. V. Grishagin *et al*., In vivo anticancer activity of rhomboidal Pt(II) metallacycles. *Proc. Natl. Acad. Sci. U.S.A.* **111**, 18448–18453 (2014).
9. Y. Sun *et al*., Melanin-dot-mediated delivery of metallacycle for NIR-II/photoacoustic dual-modal imaging-guided chemo-photothermal synergistic therapy. *Proc. Natl. Acad. Sci. U.S.A.* **116**, 16729–16735 (2019).
10. Y. Sun *et al*., Rhomboidal Pt(II) metallacycle-based NIR-II theranostic nanoprobe for tumor diagnosis and image-guided therapy. *Proc. Natl. Acad. Sci. U.S.A.* **116**, 1968–1973 (2019).
11. G. Yu *et al*., Antitumor activity of a unique polymer that incorporates a fluorescent self-assembled metallacycle. *J. Am. Chem. Soc.* **139**, 15940–15949 (2017).
12. G. Yu *et al*., Host-guest complexation-mediated codelivery of anticancer drug and photosensitizer for cancer photochemotherapy. *Proc. Natl. Acad. Sci. U.S.A.* **116**, 6618–6623 (2019).
13. H. Sepehrpour, W. Fu, Y. Sun, P. J. Stang, Biomedically relevant self-assembled metallacycles and metallacages. *J. Am. Chem. Soc.* **141**, 14005–14020 (2019).
14. Y. Sun, C. Chen, J. Liu, P. J. Stang, Recent developments in the construction and applications of platinum-based metallacycles and metallacages via coordination. *Chem. Soc. Rev.* **49**, 3889–3919 (2020).
15. S. Mura, J. Nicolas, P. Couvreur, Stimuli-responsive nanocarriers for drug delivery. *Nat. Mater.* **12**, 991–1003 (2013).
16. M. J. Webber, E. A. Appel, E. W. Meijer, R. Langer, Supramolecular biomaterials. *Nat. Mater.* **15**, 13–26 (2016).
17. M. J. Webber, R. Langer, Drug delivery by supramolecular design. *Chem. Soc. Rev.* **46**, 6600–6620 (2017).
18. P. Xing, Y. Zhao, Supramolecular vesicles for stimulus-responsive drug delivery. *Small Methods* **2**, 1700364 (2018).
19. Q. Qian, L. Zhu, X. Zhu, M. Sun, D. Yan, Drug-polymer hybrid macromolecular engineering: Degradable PEG integrated by platinum(IV) for cancer therapy. *Matter* **1**, 1618–1630 (2019).
20. W. Chen, A. Kretzschmann, W. Tian, S. Wu, Nonlinear supramolecular polymers for therapeutic applications. *Adv. Ther. (Weinh.)* **2**, 1800103 (2019).
21. W. Tian, X. Li, J. Wang, Supramolecular hyperbranched polymers. *Chem. Commun. (Camb.)* **53**, 2531–2542 (2017).
22. H. Li *et al*., Pillararene-based supramolecular polymers. *Chem. Commun. (Camb.)* **55**, 271–285 (2019).
23. M. Qi *et al*., PGMA-based supramolecular hyperbranched polycations for gene delivery. *Polym. Chem.* **7**, 4334–4341 (2016).
24. Y. Bai *et al*., Facile construction of shape-regulated β-cyclodextrin-based supramolecular self-assemblies for drug delivery. *Carbohydr. Polym.* **231**, 115714 (2020).
25. Y. Bai *et al*., Construction of β-cyclodextrin-based supramolecular hyperbranched polymers self-assemblies using AB_2-type macromonomer and their application in the drug delivery field. *Carbohydr. Polym.* **213**, 411–418 (2019).
26. M. Ikeguchi, T. Ueta, Y. Yamane, Y. Hirooka, N. Kaibara, Inducible nitric oxide synthase and survivin messenger RNA expression in hepatocellular carcinoma. *Clin. Cancer Res.* **8**, 3131–3136 (2002).
27. Y. Iwakiri, M. Y. Kim, Nitric oxide in liver diseases. *Trends Pharmacol. Sci.* **36**, 524–536 (2015).
28. V. La Mura *et al*., Liver sinusoidal endothelial dysfunction after LPS administration: A role for inducible-nitric oxide synthase. *J. Hepatol.* **61**, 1321–1327 (2014).
29. K. Machida *et al*., c-Jun mediates hepatitis C virus hepatocarcinogenesis through signal transducer and activator of transcription 3 and nitric oxide-dependent impairment of oxidative DNA repair. *Hepatology* **52**, 480–492 (2010).
30. Y. I. Moussa, J. N. Plevris, P. C. Hayes, Plasma nitrites/nitrates in HCV infection and hepatocellular carcinoma. *Eur. J. Gastroenterol. Hepatol.* **12**, 159–163 (2000).
31. M. A. Rahman *et al*., Coexpression of inducible nitric oxide synthase and COX-2 in hepatocellular carcinoma and surrounding liver: Possible involvement of COX-2 in the angiogenesis of hepatitis C virus-positive cases. *Clin. Cancer Res.* **7**, 1325–1332 (2001).
32. C.-H. Tang, W. Wei, M. A. Hanes, L. Liu, Hepatocarcinogenesis driven by GSNOR deficiency is prevented by iNOS inhibition. *Cancer Res.* **73**, 2897–2904 (2013).
33. X. Yan *et al*., Responsive supramolecular polymer metallogel constructed by orthogonal coordination-driven self-assembly and host/guest interactions. *J. Am. Chem. Soc.* **136**, 4460–4463 (2014).
34. X. Yan *et al*., Dendronized organoplatinum(II) metallacyclic polymers constructed by hierarchical coordination-driven self-assembly and hydrogen-bonding interfaces. *J. Am. Chem. Soc.* **135**, 16813–16816 (2013).
35. Z.-Y. Li *et al*., Cross-linked supramolecular polymer gels constructed from discrete multi-pillar[5]arene metallacycles and their multiple stimuli-responsive behavior. *J. Am. Chem. Soc.* **136**, 8577–8589 (2014).
36. F. Hapiot, S. Tilloy, E. Monflier, Cyclodextrins as supramolecular hosts for organometallic complexes. *Chem. Rev.* **106**, 767–781 (2006).
37. G. Yu, K. Jie, F. Huang, Supramolecular amphiphiles based on host-guest molecular recognition motifs. *Chem. Rev.* **115**, 7240–7303 (2015).
38. Y.-M. Zhang, Y.-H. Liu, Y. Liu, Cyclodextrin-based multistimuli-responsive supramolecular assemblies and their biological functions. *Adv. Mater.* **32**, e1806158 (2020).
39. S. Datta *et al*., Orthogonal self-assembly of an organoplatinum(II) metallacycle and cucurbit[8]uril that delivers curcumin to cancer cells. *Proc. Natl. Acad. Sci. U.S.A.* **115**, 8087–8092 (2018).
40. M. Zhang *et al*., Fluorescent metallacycle-cored polymers via covalent linkage and their use as contrast agents for cell imaging. *Proc. Natl. Acad. Sci. U.S.A.* **113**, 11100–11105 (2016).
41. J. Hu *et al*., Biomimetic polymers responsive to a biological signaling molecule: Nitric oxide triggered reversible self-assembly of single macromolecular chains into nanoparticles. *Angew. Chem. Int. Ed. Engl.* **53**, 7779–7784 (2014).
42. J. Hu, M. R. Whittaker, S. H. Yu, J. F. Quinn, T. P. Davis, Nitric oxide (NO) cleavable biomimetic thermoresponsive double hydrophilic diblock copolymer with tunable LCST. *Macromolecules* **48**, 3817–3824 (2015).
43. Y. Han *et al*., A biocompatible surfactant with folded hydrophilic head group: Enhancing the stability of self-inclusion complexes of ferrocenyl in a β-cyclodextrin unit by bond rigidity. *J. Am. Chem. Soc.* **128**, 13913–13920 (2006).
44. A. Harada, Y. Takashima, M. Nakahata, Supramolecular polymeric materials via cyclodextrin-guest interactions. *Acc. Chem. Res.* **47**, 2128–2140 (2014).
45. G. Thiabaud *et al*., Platinum(IV)-ferrocene conjugates and their cyclodextrin host-guest complexes. *Inorg. Chem.* **58**, 7886–7894 (2019).
46. X. Wei *et al*., Codelivery of a π–π stacked dual anticancer drug combination with nanocarriers for overcoming multidrug resistance and tumor metastasis. *Adv. Funct. Mater.* **26**, 8266–8280 (2016).
47. F. Chen *et al*., Synergistically enhanced therapeutic effect of a carrier-free HCPT/DOX nanodrug on breast cancer cells through improved cellular drug accumulation. *Mol. Pharm.* **12**, 2237–2244 (2015).
48. N. Husain, T. T. Ndou, A. M. De La Peña, I. M. Warner, Complexation of doxorubicin with β and γ-cyclodextrins. *Appl. Spectrosc.* **46**, 652–658 (1992).
49. Y. Xia *et al*., Galactose-modified selenium nanoparticles for targeted delivery of doxorubicin to hepatocellular carcinoma. *Drug Deliv.* **26**, 1–11 (2019).
50. Y. Song, C. Tang, C. Yin, Enhanced antitumor efficacy of arginine modified amphiphilic nanoparticles co-delivering doxorubicin and iSur-pDNA via the multiple synergistic effect. *Biomaterials* **150**, 1–13 (2018).